Design and Fabrication of Substrate-Free Au/SiN_X/Au Metafilm for THz Sensing Application

Zhigang Li, Yi Ou, Jianyu Fu, Wenjing Jiang, and Qing Zhao

***Abstract*—A method of designing and fabricating substrate-free Au/SiN_x/Au metafilms as the terahertz (THz) absorber of metamaterial focal plane arrays (MFPA) is reported. The absorption was investigated by the finite integration method simulation and new explicit functions. The substrate-free structure was well fabricated by microelectromechanical system (MEMS) technology. The frequency-dependent absorption of MFPA was measured by THz time-domain spectroscopy (THz-TDS) system. It exhibits an extremely high absorptance of 98.7% at 1.36 THz. The absorption characteristic shows an asymmetric profile, which is well fitted with an Asymmetric Double Sigmoidal (Asym2sig) model. Our results show that the Au/SiN_x/Au metafilms have potential in optical readout THz real-time imaging, and highly sensitive sensing applications.**

***Index Terms*—Au/SiN_x/Au metafilm, substrate-free, asymmetric peak model, THz sensing.**

I. Introduction

FOR the past 15 years, the technological development of components and the instrumentation for the largely unexplored terahertz (THz) spectral region (10^{11}–10^{13} Hz) has proceeded rapidly [1]–[3]. The THz technology has attracted considerable attention because of its unique advantages, including the strong ability of THz waves to penetrate nonpolarized objects and the fact that this region of the spectrum exhibits the characteristic absorption bands of numerous materials and molecules. The THz region has fewer harmful effects on probed persons or objects, except the associated heating effects[4], [5]. This feature gives the THz technology a significant advantage over traditional probing methods such as those employing X-rays. In addition, THz detectors are commonly used for detecting concealed objects, as well as in noninvasive medical imaging[6]–[9]. The THz technology offers a spectral window with rich scientific opportunities; however, presently, its application is limited. The lack of sensitive THz detectors is one of the main issues hindering the future development of THz technology[10], [11]. Metamaterials (MMs), which are artificial composite materials comprising subwavelength microstructures (e.g., meta-atoms, metasurfaces, metafilms) with tailored electromagnetic (EM) properties, possess arbitrary values of permittivity (ε) and permeability (μ). MMs absorbers have shown considerable application potential across numerous electromagnetic spectra, because they can tailor the frequency-dependent absorptivity[12]–[15]. Especially in the THz region, they can significantly enhance the signal detection of THz energy by adjusting the structural parameters, such as length, thickness, space, etc[16]–[18]. Therefore, they offer a promising platform for solving the above-mentioned issues[19], [20].

Integrating metafilm absorbers with bi-material cantilevers can enhance the absorption of THz energy and subsequently transfers the absorbed energy into the deformation of the bi-material cantilevers[21]–[24]. This detection unit can be arranged in an array to form a metamaterial focal plane array (MFPA), which can be used in THz real-time imaging systems [25], [26] when incorporated with an optical readout system. This optical readout imaging system has lower self-heating, longer integration times, and better signal-to-noise ratio than the electronic readout system. Alves *et al.* [21], [22], [25] reported THz SiO_2/Al bi-material cantilever sensors with Al/SiO_x/Al metafilm for THz optical readout system. The sensors operated in a frequency range >3 THz. But for THz medical imaging applications, there are many biological tissues clearly distinguished from each other in frequency less than 3 THz[27], [28]. For these requirements, a novel THz MFPA integrated with substrate-free Au/SiN_x/Au metafilms, exhibited an absorption frequency within less than 3 THz, was designed and developed in this study. The absorptance and frequency were adjusted by the thickness and patch side via the simulations respectively. For further research, the relationship between the absorptance and the thickness of the SiN_x film was investigated with a new explicit function called the revised photoluminescence (PL) intensity model[29], [30]. The measured absorption characteristic shows an asymmetrical profile, and is well fitted with an Asymmetric Double Sigmoidal (Asym2sig) peak model [31]. The two models in explicit functional form were firstly used to study the absorption properties of metafilm absorbers. They will provide a quantitative and profound understanding of the design and characteristics of the metafilm absorbers. Our results

Manuscript received March 11, 2022; revised May 29, 2022; accepted June 11, 2022. Date of publication June 15, 2022; date of current version June 28, 2022. This work was supported by the National Natural Science Foundation of China under Grants 61874137 and 61306141. *(Corresponding author: Qing Zhao.)*

Zhigang Li is with the Center for Quantum Technology Research and Key Laboratory of Advanced Optoelectronic Quantum Architecture and Measurements, School of Physics, Beijing Institute of Technology, Beijing 100081, China, and also with the Institute of Microelectronics, Chinese Academy of Sciences, Beijing 100029, China (e-mail: 3120185741@bit.edu.cn).

Qing Zhao is with the Center for Quantum Technology Research and Key Laboratory of Advanced Optoelectronic Quantum Architecture and Measurements, School of Physics, Beijing Institute of Technology, Beijing 100081, China, and also with the Beijing Academy of Quantum Information Sciences, Beijing 100193, China (e-mail: qzhaoyuping@bit.edu.cn).

Yi Ou, Jianyu Fu, and Wenjing Jiang are with the Institute of Microelectronics of the Chinese Academy of Sciences, Beijing 100029, China (e-mail: ouyi@ime.ac.cn; fujianyu@ime.ac.cn; jiangwenjing@ime.ac.cn).

Digital Object Identifier 10.1109/JPHOT.2022.3183129

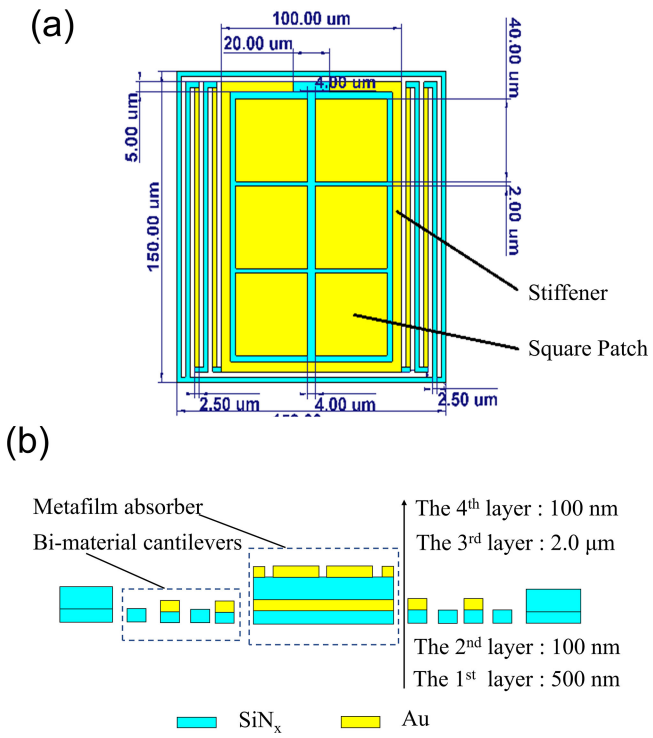

Fig. 1. (a) Top view of the MFPA pixel; (b) Cross-sectional view of the MFPA pixel.

TABLE I
PROPERTIES OF THE CONSTITUENT MATERIALS OF THE MFPA

Materials	Si	SiN_x	Au
Young's Modulus, E (GPa)	112	180	78
Expansion Coefficient, a ($10^{-6}K^{-1}$)	5.1	2.1	14
Thermal Conductivity, g ($Wm^{-1}K^{-1}$)	148	19	314
Heat Capacity, c ($JKg^{-1}K^{-1}$)	700	691	130
Density, ρ (Kgm^{-3})	2330	2400	19320
Electric Conductivity, σ ($10^{6}Sm^{-1}$)	-	-	45.61
Relative Permittivity, ε	11.9	7.5	-

TABLE II
THE BEST COEFFICIENTS TO QUANTITATIVELY INTERPRET THE ABSORPTION CHANGES WITH THE FREQUENCY OF $AU/SIN_X/AU$ AND $AL/SIO_X/AL$ WITH DIFFERENT LENGTHS

MIM metafilms	patch side (μm)	α_0	α_1	f_c THz	f_1 THz	f_2 THz	R^2
$Au/SiN_x/Au$[this work]	40	0.52	1.69	1.31	0.02	0.05	0.973
$Al/SiO_x/Al$[21]	16	0.11	3.0	4.58	0.35	0.55	0.997
	17	0.10	2.96	4.02	0.16	0.28	0.996
	18	0.12	2.82	3.73	0.15	0.27	0.989
$Al/SiO_x/Al$ [25]	14.5	0.15	2.96	4.74	0.16	0.23	0.997
	15.5	0.19	2.99	4.5	0.16	0.19	0.996
	16.5	0.14	3.0	4.14	0.15	0.22	0.995
	17.5	0.13	3.19	3.82	0.14	0.20	0.998

show that the proposed $Au/SiN_x/Au$ metafilm designs could enhance the absorptivity and achieve frequency selection. The metafilm has potential for sensing applications in optical readout THz real-time imaging, dual-wavelength spectrophotometry, and multifunction devices.

II. STRUCTURE DESIGN AND SIMULATION MODEL

Numerous studies regarding THz MMs have been reported [32]–[34]; however, these studies mainly focused on the EM response analysis of the ideal MMs. In this work, a practical microelectromechanical system (MEMS) THz MFPA with an $Au/SiN_x/Au$ metafilm absorber and bi-material cantilevers is introduced, and the absorption of the detector is particularly investigated via simulation and explicit functions. The structure of the pixel is composed of two cantilevers and an $Au/SiN_x/Au$ metafilm absorber, as shown in Fig. 1(a). The pixel size is 150×150 μm. Its cantilevers are two folded SiN_x/Au-based bi-material beams. The width of the cantilever is 2.5 μm. The absorber consists of six square patches and one stiffener. The square patch size is 40×40 μm, which is the frequency selective surface (FSS) structure. The stiffener can enhance the strength of the absorber plate. In the cross-sectional view (Fig. 1(b)) of the pixel, from bottom to top, four layers can be observed: the 1st SiN_x layer is used as the structure layer, including cantilevers and plates; the 2nd Au layer acts as a reflecting mirror for the THz radiation; the 3rd SiN_x layer is the absorption layer for the THz radiation; the 4th Au layer is used to pattern the FSS structure. The absorber features a metal-insulator-metal (MIM) configuration.

To better understand the measured response, numerical calculations based on the finite integration method were used to simulate the EM response [16], [35], [36]. The periodic nature of the MFPA structures enables the simulation to be performed in a unit cell with the appropriate boundary conditions. All full-wave numerical simulations are performed by using CST Microwave Studio software. As shown in Fig. 2(a), the FSS, MM, and a unit cell module configuration were used, and the MM unit cell was sandwiched between two air regions with Z_{max} and Z_{min} ports. Z_{max} is the incidence port; Z_{min} is the exit port. To improve the accuracy of the model, actual dimensions, including the thicknesses of the metallic layers, were used. Material properties were taken from Table I . The frequency solver allows an incident plane wave of THz radiation with a given intensity and propagation direction to penetrate a surface using scattering conditions or be generated on a boundary using ports. A perpendicular plane wave was sent through Z_{max} port1, and scattering parameters S_{11} and S_{21} were extracted over the range of the frequencies of interest. The reflectivity and transmissivity are represented by $|S_{11}|^2$ and $|S_{21}|^2$, respectively. The absorptivity of the MFPA was directly obtained using $1-|S_{11}|^2-|S_{21}|^2$. The power loss density at the specific resonant frequency of 1.36 THz is shown in Fig. 2(b). Simulations revealed that the majority of the energy is dissipated as a dielectric loss at the edge of the square patch.

For further research, we investigated the relationship between the absorption and the thickness of the SiN_x film at the expected frequency range obtained via the simulations and explicit functions. The results are considerably different from those reported by Alves *et al.* [22]. In our result, instead of a monotonic

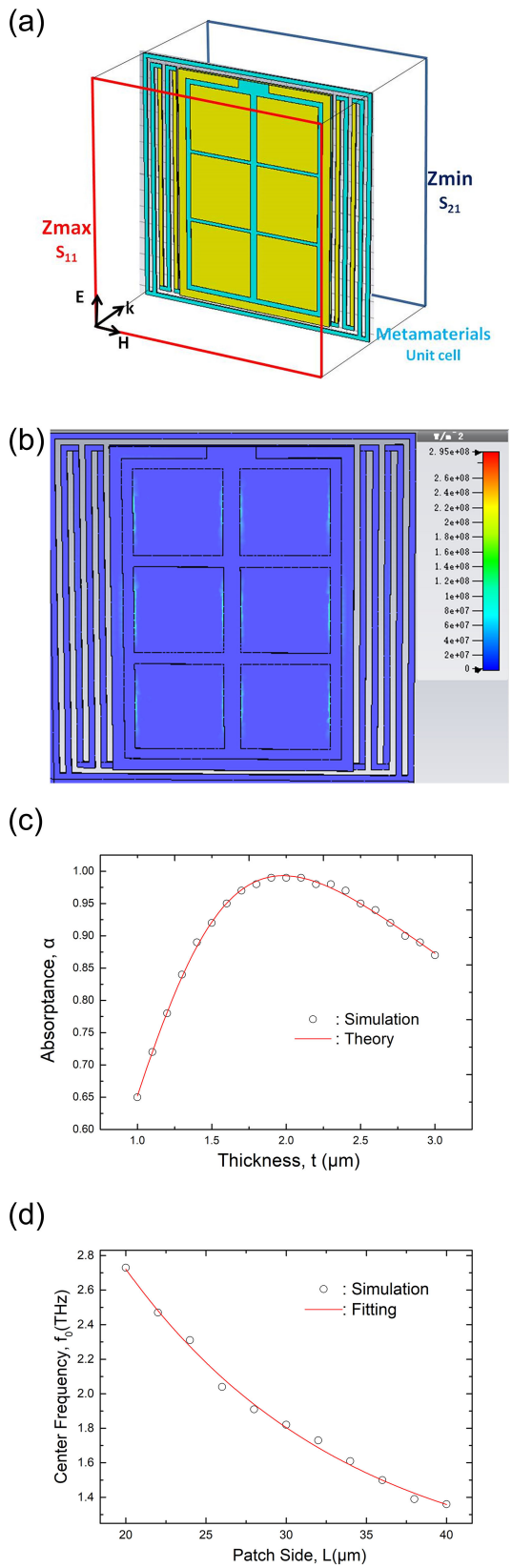

Fig. 2. (a) MM unit cell; (b) Power loss density distribution in the cell; (c) Relationship between the absorptance and the thickness of the SiN_x film; (d) Relationship between the center frequency and patch side, where the circle represents the simulation result and the red dashed line represents the fitting curve.

increase, a peak is observed in the absorption curve. We found that the PL intensity model fit well with the simulation data (Fig. 2(c)). The revised PL intensity model is expressed using (1)[29]:

$$\alpha(t) = 1.71 \times (t - 0.53)^{0.92} \times e^{\frac{0.53-t}{1.64}} \tag{1}$$

where α is the absorptance; t is the thickness of the SiN_x film. Equation (1) shows that the THz absorptance is the explicit function of the thickness of the SiN_x film. The shape of the THz absorption curve is similar to that of photoluminescence intensity. This will imply that there is some similarity between the physical mechanism of THz absorption and photoluminescence intensity.

The best value of the thickness (t_p) is derived using (2):

$$\frac{d\alpha}{dt}\Big|_{t_p} = 0 \tag{2}$$

Thus, the maximum absorptance is given by

$$t_p = 2.04\mu\text{m} \tag{3}$$

Hence, it is established that the highest theoretical absorption level is 99.36% when the film thickness is 2 μm.

The center frequency was mainly determined using the dimension of the patch array, particularly the Au patch side length. In Fig. 2(d), we present the simulation result on the relation between the center frequency and patch side, where the curve is well fitted according to a simple (4):

$$f_0 = \frac{A}{L} \tag{4}$$

where A = 54.77. In particular, when the patch side length L = 40 μm, the response center frequency f_0 = 1.36 THz, which is close to the frequency of the maximum spectral amplitude provided by the laser.

This MFPA can be applied to optical readout THz real-time imaging. The MFPAs are illuminated frontally with incident THz radiation from the target source. The absorbed THz radiation causes the temperature to increase, resulting in the deformation of the microcantilever pixels in the array. Conversely, the backside of the MFPA is illuminated with a light-emitting diode. The light reflected from the MFPA creates a thermal image and is recorded using a charge-coupled device (CCD) camera. The detection sensitivity of the optical readout system was determined by the minimum detectable angle ($\theta_{\min}$), corresponding to one gray level of CCD. It can be expressed as follows[23]:

$$\theta_{\min} = \frac{\Delta\theta}{\Delta I} = \frac{\lambda}{2L_r N} \tag{5}$$

where λ is the wavelength of the readout light, L_r is the reflector length along the cantilever direction, N is the quantization level of the CCD, $\Delta\theta$, and ΔI are the changes in the deformation angle and the gray level of the CCD, respectively. Therefore, the reflector length along the leg must be as long as possible to minimize $\theta_{\min}$. The reflector length is easy to be longer via integrating more patches. So, this MFPA with the Au/SiN_x/Au metafilm absorber may achieve highly sensitive THz detector.

III. Results and Discussions

All the samples were prepared using MEMS fabrication processes, as shown in Fig. 3(a). The fabrication procedure is as follows: a) a 5000-Å thick low-pressure chemical vapor deposition (LPCVD) SiN_x layer is generated on double sides of the wafer; b) a 1000-Å thick gold layer is evaporated on the front side, and 2.0 μm of the PECVD SiN_x layer is deposited on top of the gold layer; c) lithography and reactive ion etching (RIE) are performed to open the back etching window; d) front lithography and RIE are performed to pattern the absorption layer below the FSS structure; e) a gold layer is etched; f) the cantilevers are etched; g) the cantilevers and the FSS structure are patterned by gold evaporation; h) the pixel is released by backside silicon wet etching. The MFPAs were fabricated on a four-inch silicon wafer using 2×2 cells, as shown in Fig. 3(b). The obtained MFPA has a dimension of 1.5×1.5 cm and holds 100×100 pixels. The structure of the fabricated pixels was inspected by scanning electron microscope (SEM) and 3D optical microscope. From the SEM image shown in Fig. 3(c), the substrate-free Au/SiN_x/Au metafilm structure is well fabricated. Fig. 3(d) shows the three-dimensional (3D) shape of the pixels with initial deformation. The blue area is tilted up and the red area is tilted down.

Finally, the MFPA absorption was measured using a THz time-domain spectroscopy system (THz-TDS), as shown in Fig. 4(a). The THz wave was generated using a low-temperature grown GaAs photoconductive antenna integrated with a Si hemisphere lens. A beam of p-polarized Ti: sapphire femtosecond laser (Maitai Spectra-physics; repetition rate: 80 MHz; pulse width: 70 fs; central wavelength: 800 nm; averaged power: 30 mW) was employed as the excitation source. Next, a parabolic mirror was used to collimate the pulse and to direct it toward the THz MFPA under study. THz detection was realized using a ZnTe crystal via electro-optical sampling [37]. The incident angle of the THz beam was fixed at 30°. Both the transmitted and reflected THz waves were measured, and then the absorption equates to 1-R-T, where reflectivity and transmissivity are given by R and T. As depicted in Fig. 4(b), the absorption peak of 98.7% is found at 1.36 THz. And the absorption characteristic shows an asymmetrical profile. To interpret the characteristic, we propose an asymmetric peak model known as Asym2sig. The Asym2sig peak model with five parameters is written as follows [31], [38]:

$$\alpha(f) = \alpha_0 + \frac{\alpha_1}{1 = \exp((f_c - f/f_1)} \times \left[1 - \frac{1}{1 + \exp((f_c - f)/f_2)}\right] \quad (6)$$

where α_0 is the vertical offset absorption, α_1 is the maximum amplitude absorption coefficient, f_c is the horizontal center position frequency, and f_1 and f_2 are the shape parameters that determine the asymmetry peak level. The best-fitting model parameters α_0, α_1, f_c, f_1, and f_2, were anticipated using the nonlinear least-squares curve regression analysis method. The Asym2sig peak model (6) was evaluated by R^2 as the coefficient of determination (Table II). The nonlinear least squire curve

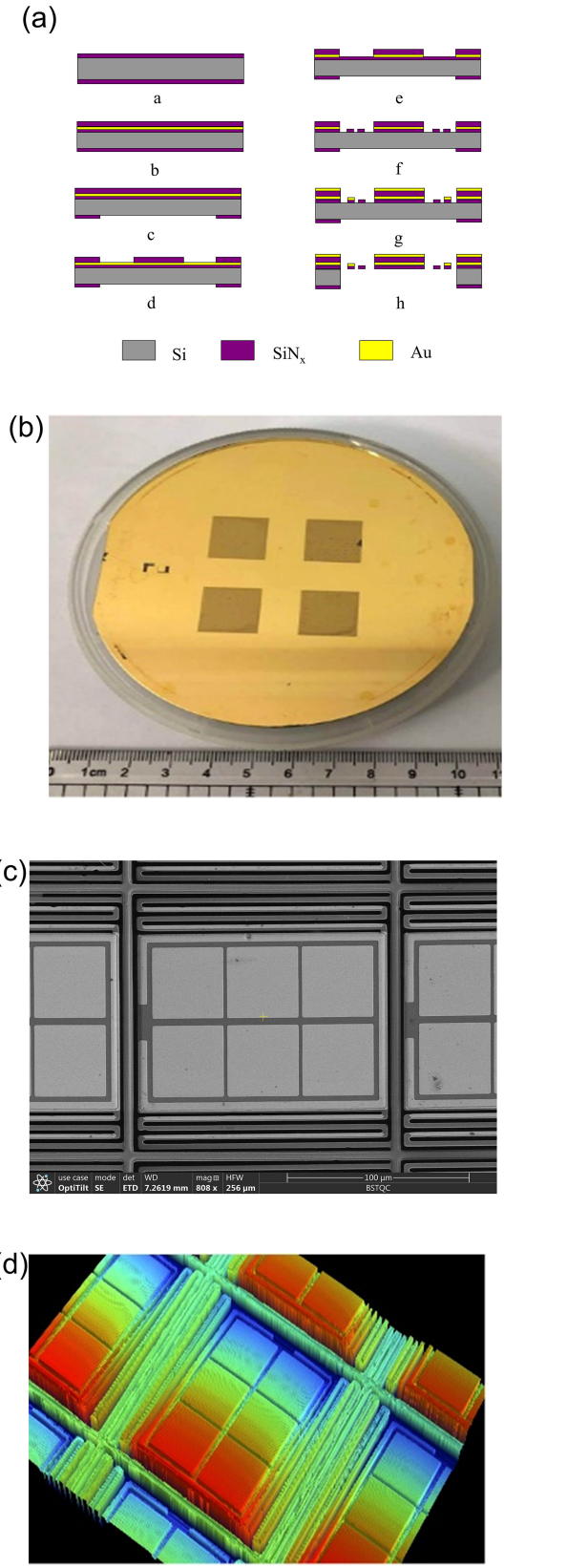

Fig. 3. (a) Fabrication flowchart of the MEMS MFPA; (b) Photograph of four fabricated MFPAs on a 4-inch silicon wafer; (c) SEM image of the pixels; (d) 3D shape of the pixels.

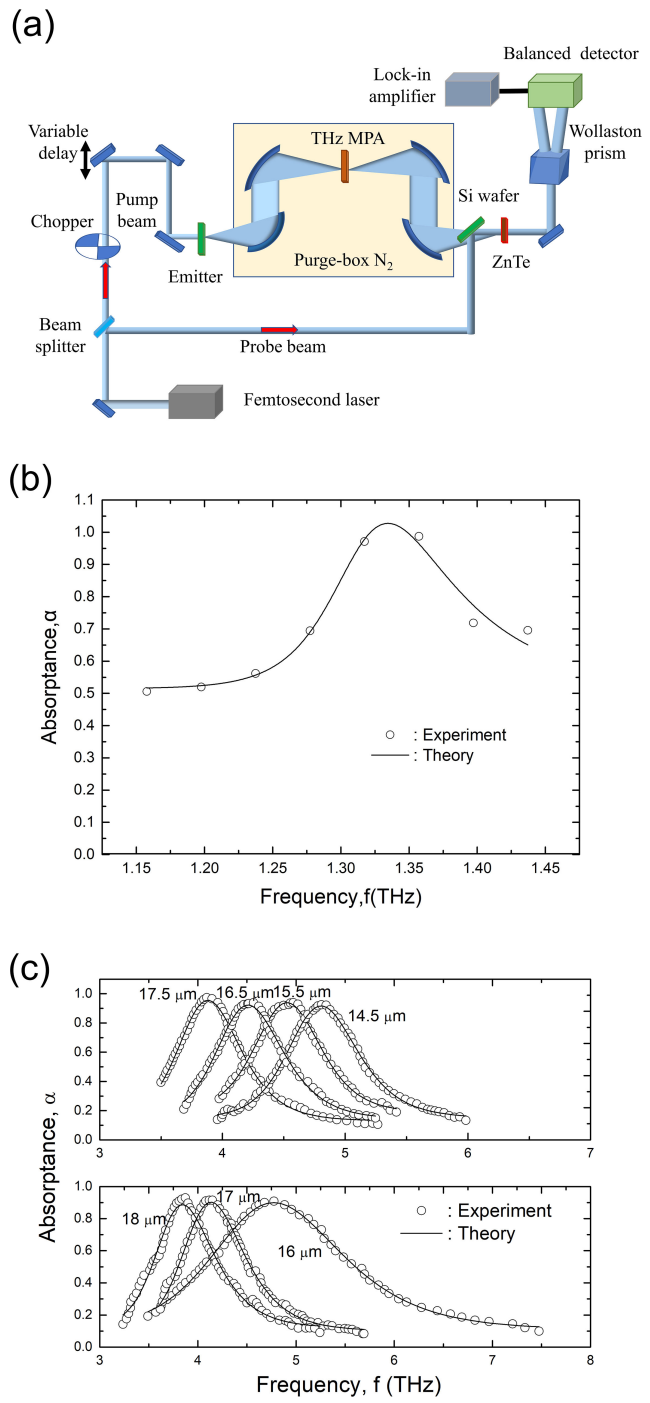

Fig. 4. (a) Schematic of the THz-TDS employed to measure both the reflectance and transmittance; (b) Experiment (circle) and Asym2sig model (6) fitting (solid lines) absorption against frequency; (c) Comparison between the experiment measurement (circle) [21], [25] and Asym2sig model (6) fitting (solid lines).

fitting of the Asym2sig model on experimental data was also shown in Fig. 4(b). The high R^2 ($= 0.973$) value reveals a good agreement between the experiment and fitting results.

To verify the universality of the Asym2sig model (6), parameter estimation from the third part of the experimental data is critical to the desired model. The experimental absorption-frequency data at the different length of the Al/SiO$_x$/Al metafilm absorber were taken from the papers [21], [25]. The theoretical curves of absorption-frequency were obtained after the nonlinear least squire curve fitting of the Asym2sig model (6) on experimental data and shown in Fig. 4(c). The model fits well with the experimental data. The best coefficients of Asym2sig fitting in each experimental curve are listed in Table II, where α_0 and α_1 are the absorptions, characterizing the caption of THz absorption. The confidence level of each parameter is above 0.99.

IV. Conclusion

A 100×100 THz MFPA with Au/SiN$_x$/Au metafilm absorbers array and bi-material cantilevers is designed, fabricated, characterized, and subjected to theoretical simulations. The MFPA pixel dimension is 150 × 150 μm with a substrate-free structure. An extremely high absorption ratio is characterized by THz-TDS. The fabricated MFPA exhibits a 98.7% resonant absorption at 1.36 THz, agreeing well with the theoretical results. The THz absorptance characteristics are investigated by performing simulation studies and using a revised PL intensity model and an asymmetric Asym2sig model. The relationship between the absorptance, the thickness of the SiN$_x$ film, and the size of the square patch is theoretically analyzed. The results show that these theoretical models enable the application of theoretical analysis to the MIM absorbers. Our results prove that this substrate-free THz MFPA and analysis methods have various applications in THz technology, e.g., in dual-wavelength spectrophotometry and THz imaging.

Acknowledgment

The authors would like to thank Dr. Bo Wang for the THz measurement.

References

[1] M. Choi *et al.*, "A terahertz metamaterial with unnaturally high refractive index," *Nature*, vol. 470, no. 7334, pp. 369–373, 2011, doi: 10.1038/nature09776.
[2] Q. Li *et al.*, "Subterahertz collective dynamics of polar vortices," *Nature*, vol. 592, no. 7854, pp. 376–380, 2021, doi: 10.1038/s41586-021-03342-4.
[3] K. Peng *et al.*, "Three-dimensional cross-nanowire networks recover full terahertz state," *Science*, vol. 368, no. 6490, pp. 510–513, 2020, doi: doi: 10.1126/science.abb0924.
[4] N. I. Zheludev and Y. S. Kivshar, "From metamaterials to metadevices," *Nature Mater.*, vol. 11, no. 11, pp. 917–924, 2012, doi: 10.1038/nmat3431.
[5] L. Liebermeister *et al.*, "Optoelectronic frequency-modulated continuous-wave terahertz spectroscopy with 4 THz bandwidth," *Nature Commun.*, vol. 12, no. 1, 2021, Art. no. 1071, doi: 10.1038/s41467-021-21260-x.
[6] N. Kanda, K. Konishi, N. Nemoto, K. Midorikawa, and M. Kuwata-Gonokami, "Real-time broadband terahertz spectroscopic imaging by using a high-sensitivity terahertz camera," *Sci. Rep.*, vol. 7, no. 1, 2017, Art. no. 42540, doi: 10.1038/srep42540.
[7] M. Gupta *et al.*, "Sharp toroidal resonances in planar terahertz metasurfaces," *Adv. Mater.*, vol. 28, no. 37, pp. 8206–8211, 2016, doi: https://doi.org/10.1002/adma.201601611.
[8] L. A. Sterczewski *et al.*, "Terahertz hyperspectral imaging with dual chip-scale combs," *Optica*, vol. 6, no. 6, pp. 766–771, 2019, doi: 10.1364/OPTICA.6.000766.
[9] R. I. Stantchev, X. Yu, T. Blu, and E. Pickwell-MacPherson, "Real-time terahertz imaging with a single-pixel detector," *Nature Commun.*, vol. 11, no. 1, 2020, Art. no. 2535, doi: 10.1038/s41467-020-16370-x.

[10] X. C. Zhang, A. Shkurinov, and Y. Zhang, "Extreme terahertz science," *Nature Photon.*, vol. 11, no. 1, pp. 16–18, 2017, doi: 10.1038/nphoton.2016.249.

[11] X. J. Ying Tian, Haiyong Gan, Chenxia Li, and Zhi Hong, "Free control of far-field scattering angle of transmission terahertz wave using multilayer split-ring resonators' metasurfaces," *Front. Phys.*, vol. 15, no. 6, 2020, Art. no. 62502, doi: 10.1007/s11467-020-1013-1.

[12] W. Wang *et al.*, "Enhancing sensing capacity of terahertz metamaterial absorbers with a surface-relief design," *Photon. Res.*, vol. 8, no. 4, pp. 519–527, 2020, doi: 10.1364/PRJ.386040.

[13] Z. Shen, S. Li, Y. Xu, W. Yin, L. Zhang, and X. Chen, "Three-dimensional printed ultrabroadband terahertz metamaterial absorbers," *Phys. Rev. Appl.*, vol. 16, no. 1, 2021, Art. no. 014066, doi: 10.1103/PhysRevApplied.16.014066.

[14] C. Liu, Y. Xu, H. Liu, M. Lin, and S. Zha, "Switchable metamaterial with terahertz buffering and absorbing performance," *IEEE Photon. J.*, vol. 13, no. 5, May 2021, Art. no. 4600408, doi: 10.1109/JPHOT.2021.3107533.

[15] V. S. Yadav, B. K. Kaushik, and A. Patnaik, "Broadband THz absorber for large inclination angle TE and TM waves," *IEEE Photon. J.*, vol. 13, no. 5, May 2021, Art. no. 7700107, doi: 10.1109/JPHOT.2021.3112550.

[16] C. Chen *et al.*, "Ultrathin terahertz triple-band metamaterial absorbers: Consideration of interlayer coupling," *Phys. Rev. Appl.*, vol. 14, no. 5, 2020, Art. no. 054021, doi: 10.1103/PhysRevApplied.14.054021.

[17] J. P. del Risco *et al.*, "Optimal angular stability of reflectionless metasurface absorbers," *Phys. Rev. B*, vol. 103, no. 11, 2021, Art. no. 115426, doi: 10.1103/PhysRevB.103.115426.

[18] S. Barzegar-Parizi, A. Ebrahimi, and K. Ghorbani, "Dual-broadband and single ultrawideband absorbers from the terahertz to infrared regime," *J. Opt. Soc. Amer. B*, vol. 38, no. 9, pp. 2628–2637, 2021, doi: 10.1364/JOSAB.432329.

[19] S. Sun, Q. He, J. Hao, S. Xiao, and L. Zhou, "Electromagnetic metasurfaces: Physics and applications," *Adv. Opt. Photon.*, vol. 11, no. 2, pp. 380–479, 2019, doi: 10.1364/AOP.11.000380.

[20] H.-L. Jiang, J. Pan, W. Zhou, H.-M. Li, and S. Liu, "Fabrication and application of arrays related to two-dimensional materials," *Rare Met.*, vol. 41, no. 1, pp. 262–286, 2022, doi: 10.1007/s12598-021-01842-w.

[21] F. Alves, D. Grbovic, B. Kearney, N. V. Lavrik, and G. Karunasiri, "Bi-material terahertz sensors using metamaterial structures," *Opt. Exp.*, vol. 21, no. 11, pp. 13256–13271, 2013, doi: 10.1364/OE.21.013256.

[22] F. Alves, B. Kearney, D. Grbovic, N. V. Lavrik, and G. Karunasiri, "Strong terahertz absorption using SiO_2/Al based metamaterial structures," *Appl. Phys. Lett.*, vol. 100, no. 11, 2012, Art. no. 111104, doi: 10.1063/1.3693407.

[23] Y. Ou, Z. Li, F. Dong, D. Chen, Q. Zhang, and C. Xie, "Design, fabrication, and characterization of a 240 $\times$ 240 MEMS uncooled infrared focal plane array with 42 μm pitch pixels," *J. Microelectromech. Syst.*, vol. 22, no. 2, pp. 452–461, 2013, doi: 10.1109/JMEMS.2012.2227140.

[24] X. Zhao, G. Duan, A. Li, C. Chen, and X. Zhang, "Integrating microsystems with metamaterials towards metadevices," *Microsyst. Nanoeng.*, vol. 5, no. 1, 2019, Art. no. 5, doi: 10.1038/s41378-018-0042-1.

[25] F. Alves, L. Pimental, D. Grbovic, and G. Karunasiri, "MEMS terahertz-to-infrared band converter using frequency selective planar metamaterial," *Sci. Rep.*, vol. 8, no. 1, Aug. 2018, Art. no. 12466, doi: 10.1038/s41598-018-30858-z.

[26] Y. Jin, H. Shi, and Q. Zhang, "Optical spatial filtering readout techniques for IR/THz imaging and their performance analysis," *Meas. Sci. Technol.*, vol. 32, no. 6, 2021, Art. no. 065202, doi: 10.1088/1361-6501/abc1af.

[27] H. Lindley-Hatcher, R. I. Stantchev, X. Chen, A. I. Hernandez-Serrano, J. Hardwicke, and E. Pickwell-MacPherson, "Real time THz imaging—Opportunities and challenges for skin cancer detection," *Appl. Phys. Lett.*, vol. 118, no. 23, 2021, Art. no. 230501, doi: 10.1063/5.0055259.

[28] Z. Yan, L.-G. Zhu, K. Meng, W. Huang, and Q. Shi, "THz medical imaging: From in vitro to in vivo," *Trends Biotechnol.*, vol. 40, no. 7, pp. 816–830, 2022, doi: 10.1016/j.tibtech.2021.12.002.

[29] S. Sabri, A. Faraji, R. Malek, and K. Kassmi, "Photoluminescence (PL) characterization of InAs/GaAs quantum dots (QDs): A theoretical study," in *Proc. Int. Conf. Mater. Environ. Sci.*, 2020.

[30] L. Changshi, "Prediction of the photoluminescence of In0.53Ga0.47As/InP irradiated by 1MeV electron," *Nucl. Instruments Methods Phys. Res. Sect. B: Beam Interact. Mater. At.*, vol. 391, pp. 64–68, 2017, doi: 10.1016/j.nimb.2016.11.003.

[31] C. Chen, W. Miao, C. Zhou, and H. Wu, "Thermogravimetric pyrolysis kinetics of bamboo waste via asymmetric double sigmoidal (Asym2sig) function deconvolution," *Bioresource Technol.*, vol. 225, pp. 48–57, 2017, doi: 10.1016/j.biortech.2016.11.013.

[32] T. Kan *et al.*, "Enantiomeric switching of chiral metamaterial for terahertz polarization modulation employing vertically deformable MEMS spirals," *Nature Commun.*, vol. 6, no. 1, 2015, Art. no. 8422, doi: 10.1038/ncomms9422.

[33] A. Karvounis *et al.*, "Mechanochromic reconfigurable metasurfaces," *Adv. Sci.*, vol. 6, no. 21, 2019, Art. no. 1900974, doi: 10.1002/advs.201900974.

[34] M. Manjappa *et al.*, "Reconfigurable MEMS fano metasurfaces with multiple-input–output states for logic operations at terahertz frequencies," *Nature Commun.*, vol. 9, no. 1, 2018, Art. no. 4056, doi: 10.1038/s41467-018-06360-5.

[35] S. Wang *et al.*, "Vanadium dioxide based broadband THz metamaterial absorbers with high tunability: Simulation study," *Opt. Exp.*, vol. 27, no. 14, pp. 19436–19447, 2019, doi: 10.1364/OE.27.019436.

[36] Y. Zhou *et al.*, "Ultra-broadband metamaterial absorbers from long to very long infrared regime," *Light: Sci. Appl.*, vol. 10, no. 1, 2021, Art. no. 138, doi: 10.1038/s41377-021-00577-8.

[37] Y. Zhou *et al.*, "Terahertz wave reflection impedance matching properties of graphene layers at oblique incidence," *Carbon*, vol. 96, pp. 1129–1137, 2016, doi: 10.1016/j.carbon.2015.10.063.

[38] J. L. F. Alves *et al.*, "Determination of the bioenergy potential of brazilian pine-fruit shell via pyrolysis kinetics, thermodynamic study, and evolved gas analysis," *BioEnergy Res.*, vol. 12, no. 1, pp. 168–183, 2019, doi: 10.1007/s12155-019-9964-1.